



# Laser-based thermomechanical joining of semi-transparent thermoplastics with technical steel

Silvio Genna<sup>1</sup> · Patrizia Moretti<sup>1</sup> · Gennaro Salvatore Ponticelli<sup>2</sup> · Simone Venettacci<sup>2</sup>

Received: 28 February 2024 / Accepted: 10 April 2024 / Published online: 16 April 2024  
© The Author(s), under exclusive licence to Springer-Verlag London Ltd., part of Springer Nature 2024

## Abstract

The laser-based thermomechanical joining process was adopted to produce hybrid components made of AISI 304 stainless steel and semi-transparent thermoplastic materials, i.e. polypropylene and polyamide. The process parameters, i.e. laser power, laser-polymer interaction time, and metal surface texture, were optimized using the full factorial experimental approach, and the joints' quality and performance were examined to determine the best operational parameters' combination. Shear tests were carried out to evaluate the resistance of the joints, while morphological and fracture surface analyses were performed to have a better understanding of the phenomena that emerged during the joining process. The findings demonstrated that the shear force and the joint area were significantly influenced primarily by the texture, followed by the laser power, and finally the interaction time. The optimal combination allowed the realization of joints whose maximum shear force reached around 750 N for polypropylene and around 2200 N for polyamide, achieving respectively 60% and 53% of the tensile force of the polymer base materials.

**Keywords** Laser joining · Diode laser · Stainless steel · Thermoplastic · Surface texturing · Interlocking mechanism

## 1 Introduction

Thermomechanical joining of thermoplastic materials with technical metals is emerged as a modern solution to produce hybrid components without joining elements or adhesives to simplify the manufacturing process steps and thus reduce production time and costs [1]. In fact, mechanical fastening generally involves external elements, which require relatively extensive pre-treatments (e.g. making holes) and increase the weight and the cost of the structure [2]. Moreover, there is a stress concentration where the element is fastened [3]. While employing adhesives results in a better distribution of stresses, there are drawbacks such as time-consuming curing processes, environmental vulnerability, long-term instability, and high sensitivity to loading direction [4]. As a consequence, joints are the most common source of premature in-service failure for hybrid structures

[5]. In this light, regardless of the adopted solution, joints represent one of the greatest challenges in the design of hybrid structures for those sectors that simultaneously seek for structural integrity, reduction of weight, and simplification of the joining process for low-cost and efficient production, e.g. infrastructure, transportation, automotive, aeronautics, and aerospace [6].

Unlike the traditional methods, thermomechanical joining processes involve local heating using different sources, from lasers [7, 8], to friction [9, 10], ultrasound [11, 12], injection moulding [13, 14], etc., while applying a compression, to join polymer and metal parts in a lap-joint configuration [3]. More recently, new concepts of these processes have addressed the possibility of joining the polymer on a surface-structured metal [14, 15]. This allows for an improved interlocking through the thickness of the metal substrate, enhancing the joint's out-of-plane strength [6], therefore overcoming the poor chemical affinity between these materials which prevent the chemical bonding. Among these solutions, the laser-based thermal process shows advantages due to several reasons, among which the most notable ones are the possibility to focus the energy input to a limited region, allowing for the processing of small and/or complex-shaped parts [16, 17], and that laser systems can be adopted

✉ Gennaro Salvatore Ponticelli  
gennaro.ponticelli@unicusano.it

<sup>1</sup> Department of Enterprise Engineering, University of Rome Tor Vergata, Via del Politecnico 1, 00133 Rome, Italy

<sup>2</sup> Department of Engineering, University of Rome Niccolò Cusano, Via Don Carlo Gnocchi 3, 00166 Rome, Italy

to perform different operations, i.e. measurements [18] and treatments [19], ensuring flexibility and suitability for automation [20].

The procedure to join the thermoplastic and the metal substrate can be carried out as heat conduction or transmission joining. When combining materials using transmission joining, the laser beam passes through the polymer before reaching the metal surface, where it is partially absorbed. Through heat transmission at the interface, the polymer melts and creates a joint, while in heat conduction joining, the laser beam is directed towards the surface of the metal substrate and the heat is transferred into the connecting zone and boundary layer through the metal itself. Laser transmission joining is used with materials that transmit near infrared radiation, notably polymers [21], and nowadays is one of the most promising solutions for joining hybrid structures made of transparent or semi-transparent polymers and other materials [22]. Among lasers, those operating in the wavelength range of 0.8 to 1.1  $\mu\text{m}$  are often employed for joining processes of natural polymers since these have a low absorption in such spectral area up to several millimetres of thickness [23]. Typical systems adopt diode, fibre, or Nd:YAG lasers, in favour of the first ones given their low purchase costs, high energy efficiency (around 40%), and flat energy distribution [24]. This last characteristic represents a notable advantage in joining operations involving polymer materials, as high focusing is not required, while the polymer must reach the molten state remaining below the decomposition temperature [22, 25].

Previous studies have highlighted that many factors can influence the joining process and therefore the resulting joint strength of metal-polymer hybrid structures, i.e. laser power, laser-polymer interaction time (or welding speed), number of scans, laser beam diameter, clamp pressure, laser wavelength, and defocus distance. Among these, the first two are considered the main controlling parameters as they control the heat input and heat diffusion during the laser joining process [21, 26]. In addition, the nature of the polymer, the chemical composition of the metal substrate, and the morphology of the metal surface also affect the resulting joint strength [3]. Wang et al. [27] investigated the effect of laser power and welding speed on the joint strength between 304 stainless steel and PET, highlighting a threshold value of 15 mm/s, with a maximum resistance at around 2 kN, i.e. 79% of the strength of the base material, beyond which the performance deteriorates. Elahi and Plapper [28] verified the effect of different surface textures obtained on 304 stainless steel substrates to be joined with PA, showing that all the solutions provided a higher shear load of the hybrid components compared to the untreated ones, up to around 2.1 kN, against the initial 1.3 kN. Wu et al. [29] successfully joined 316L stainless steel and PLA for varying values of laser power, pulse duty ratio, and welding speed, obtaining

a maximum shear force of around 1.7 kN, i.e. around 77% of the tensile force of the base material. Adarsh and Natarajan [30] studied the laser joining process of AA5754 aluminium alloy and PA by controlling the laser power, the welding speed, and the defocus distance, finding that the optimal condition, i.e. 1.6 kW, 2.4 mm/s, and 9 mm, respectively, allowed for a shear force of around 1 kN, which increased at around 1.6 kN by modifying the surface texture of the metal substrate. However, the maximum tensile lap shear load was around 40% of that of the polymer base material shear failure load. Temesi and Czigany [31] determined the effect of the surface morphology of AA6082 aluminium alloy substrate to be joined with PP, highlighting that the higher the number of grooves of the texture, the greater the shear force, up to around 1.25 kN, which is 72.5% of the strength of the base material used.

From the literature analysis, it is clear that there is a very large number of polymer-metal combinations and process parameters currently being studied to find the optimal condition to successfully obtain a performing and repeatable hybrid joint through laser-based thermomechanical joining processes. In order to achieve optimal joint quality in a cost-effective manner and to gain a greater understanding of process mechanics and parametric effects, the optimization of such processes is thus a priority topic, leading to additional research on these aspects [25]. In this context, the present study deals with the optimization of the laser-based thermomechanical joining of semi-transparent thermoplastics, i.e. polypropylene (PP) and polyamide (PA66), with technical steel, i.e. AISI 304 stainless steel, whose surface has been appropriately textured by adopting the same laser system for the joining process. Shear force, shear strength, joint surface, joint morphology, and failure modes were classified to provide a feasible method for joining through the control of laser power, laser-polymer interaction time, and surface texture of the metal substrate.

## 2 Experimental procedure

In this research work, two semi-transparent commercial polymer materials, i.e. polypropylene (PP) and nylon grade 66 (PA66), were joint through laser irradiation with a metal substrate, i.e. AISI 304 stainless steel (SS304), to define the optimal process windows to obtain durable polymer/metal hybrid joints. The investigation concerned three main activities, as shown in Fig. 1. The following is a short summary:

- i. The first activity covered the preliminary characterization of the polymers by evaluating their mechanical and thermal properties; the former concerned the execution of static tensile tests, while the latter the study of the degradation properties of the materials

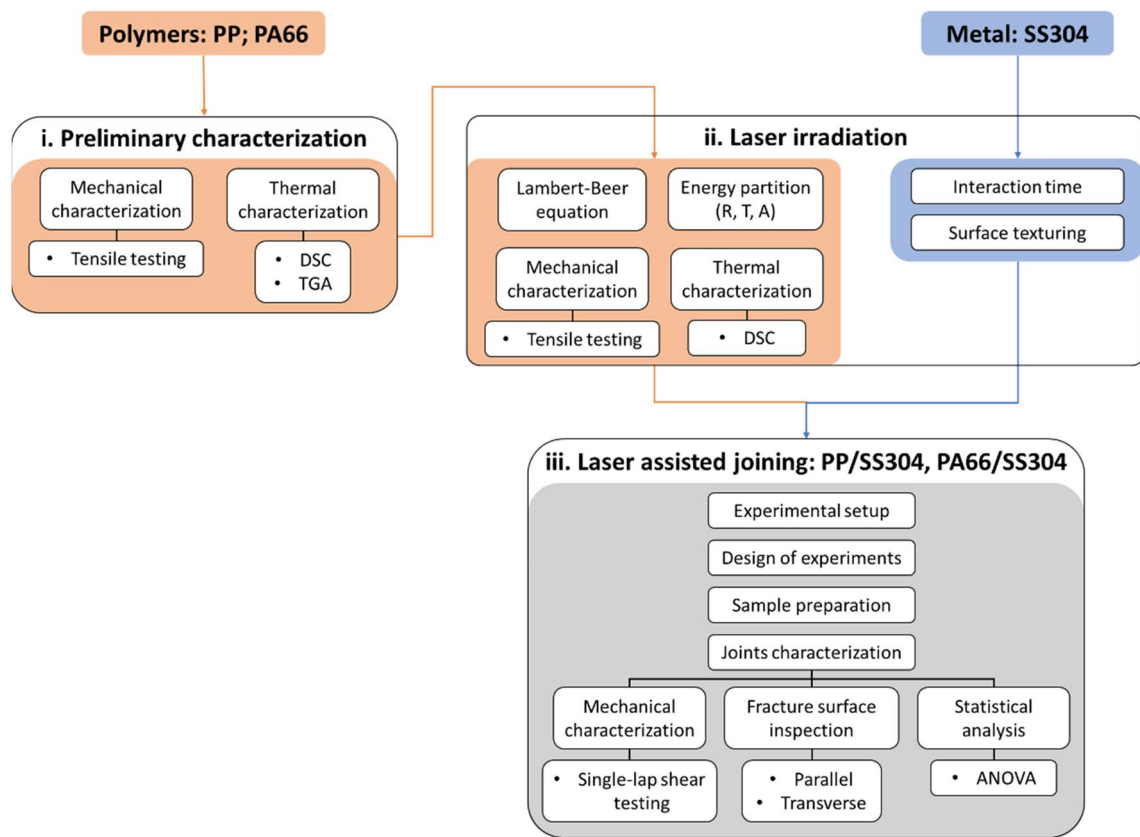


Fig. 1 Flowchart of the activities carried out for the realization of laser-assisted metal/polymer joints

through differential scanning calorimetry (DSC) and thermogravimetric analysis (TGA) to properly tune the laser processing parameters for irradiation.

- ii. The second step was aimed at investigating the interaction mechanisms between the laser and the materials; for polymers, the Lambert-Beer equation and the energy partition, in terms of reflected (R), transmitted (T), and absorbed (A) energy, were evaluated. Moreover, DSC and static tensile tests were conducted to identify any modification induced by the laser treatment on both thermal and mechanical properties. While for the SS304, this activity concerned the estimation of the optimal laser irradiation time and laser power to avoid the polymers’ degradation and the realization of three different surface textures with the aim to improve the mechanical bonding between the materials during joining.
- iii. After the realization of the experimental setup to join the materials, based on the results of the previous steps, according to an *ad hoc* experimental plan developed on the basis of Design of Experiments, the samples were prepared and adopted in single-lap shear tests to study the strength of the joints. The resulting fracture surfaces were inspected through opti-

cal microscopy observing both the parallel and the transverse surfaces. Finally, the results were analyzed through the analysis of variance (ANOVA) statistical method.

## 2.1 Materials

The polymer materials adopted are commercial extruded polypropylene and nylon (grade 66) sheets 3 mm and 6 mm thick, respectively, supplied by RS Components, code 682-551 for PP and 704-8144 for PA66. The main characteristics are summarized in Table 1. It is worth noting that the experimental campaign concerned the estimation of these properties to have a proper comparison before and after the laser treatment due to the range variation, as detailed in the

Table 1 Mechanical properties of materials as declared by the suppliers

Material	Polypropylene	Nylon 66	AISI 304
Ultimate tensile strength, MPa	27–30	60–80	535
Young’s modulus, GPa	1.6–2.0	3.4	197
Elongation at break, %	10–50	150	65

following sections. These polymers were then bonded to rolled AISI 304 stainless steel sheets 1 mm thick, whose characteristics are listed in Table 1.

## 2.2 Sample preparation

The samples adopted during this research work were obtained from the available slabs using the STEPCRAFT D840 numerical control machine equipped with a  $\varnothing 2$  mm 828 burr supplied by MJ CNC Automation. The cutting parameters were properly chosen to guarantee the best quality of the lateral surface together with the maximum production rate: the cutting speed was set at 17000 rpm, the depth of cut at 3 mm (1 pass for PP and 2 passes for PA66), while the feed rate at 1200 mm/min and 1000 mm/min for PP and PA66, respectively. Please refer to Section 2.4 for the geometry of the samples.

## 2.3 Thermal characterization

The thermal characterization concerned two main steps: (i) the identification of the main thermal properties through differential scanning calorimetry and (ii) the evaluation of the degradation of the polymers with the temperature through the thermogravimetric analysis. The definition of the melting temperature, through DSC, together with the measurement of the degradation temperature, through TGA, represents the two main factors to correctly set the laser parameters to be used during the joining process, as to guarantee better fluidity of the polymer within the asperities of the metal substrate and to avoid its degradation.

The DSC allows the estimation of the main thermal properties of the polymers, i.e. melting temperature ( $T_m$ , °C), crystallization temperature ( $T_c$ , °C), glass transition temperature ( $T_g$ , °C), and degree of crystallinity ( $X_c$ , %). The tests were conducted using the DSC Q2000 by TA Instruments by setting a heating/cooling speed of 10 °C/min, a nitrogen flow of 20 mL/min, and a temperature interval dependent on the specific material, as reported in Table 2. The choice of these intervals was made on the basis of the literature data. The cycle was repeated twice. It is worth noting that the degree of crystallinity was calculated according to Eq. (1), where  $\Delta H_m$  is the melting enthalpy of the material measured at the melting temperature, as the area subtended by the characteristic melting peak of the DSC diagram, and

$\Delta H_0$  is the melting enthalpy of the 100% crystalline material at the equilibrium melting temperature [37], whose values are listed in Table 2. The samples consisted of 5 to 10 mg of material placed in an aluminium crucible. The tests were carried out before and after the laser treatment to evaluate any modification induced by the laser irradiation.

$$X_c = \frac{\Delta H_m}{\Delta H_0} 100 \quad (1)$$

The degradation mechanisms of the polymers were studied by thermogravimetric analysis during the preliminary characterization. This technique measures the mass variation of the polymer as a function of temperature or time, appropriately controlled, through the use of a thermobalance. The system adopted for this study is the Perkin Elmer Pyris Diamond TGA. The samples were heated from a temperature of 25 °C up to 800 °C in nitrogen flow of 100 mL/min at a rate of 10 °C/min. The samples consisted of 8 to 10 mg of material placed in a ceramic crucible. This analysis allows to determine the degradation state of the polymer through the evaluation of three main characteristics, as schematized in Fig. 2: (i) the peak temperature of the first derivative of the TGA curve ( $T_{DTG}$ , °C), indicated as DTG, represented with a black dotted line and quantified in  $\mu\text{g}/\text{min}$ . It indicates the point of greatest rate of change on the weight loss, corresponding to the inflexion point of the TGA curve; (ii) the extrapolated onset temperature ( $T_{on,E}$ , °C), evaluated according to the ISO 11358-1 standard as the intersection point of the initial mass baseline and the tangent to the TGA curve at the point of maximum slope. It is considered the maximum temperature above which the degradation phenomenon definitively compromises the sample [38]; (iii) the percentage of material residue after the test ( $R_m$ , %).

## 2.4 Mechanical characterization

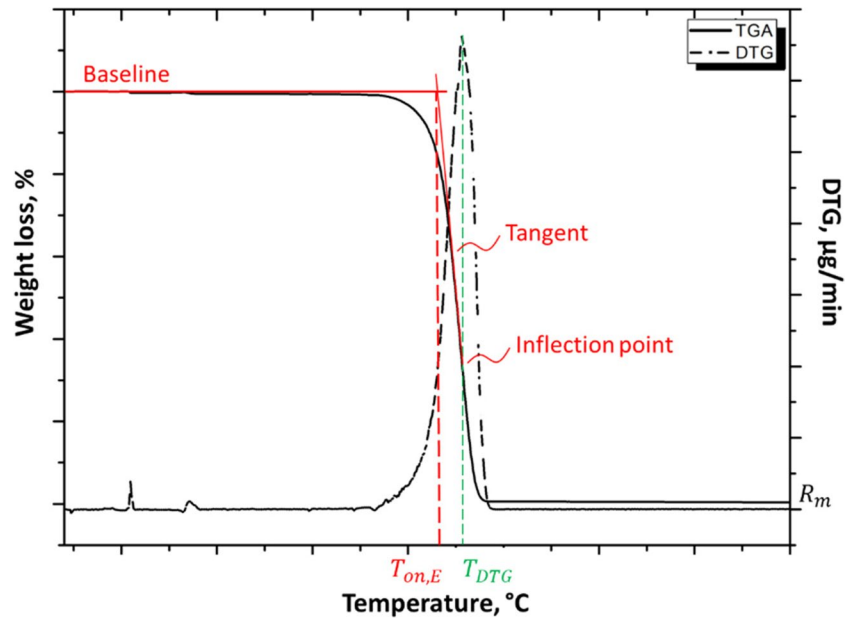
The characterization of the mechanical properties of the polymer materials was carried out before and after the laser irradiation to identify any change induced by the thermal treatment. Such investigations were performed through static tensile tests. Moreover, after the joining process, the obtained specimens were characterized by means of single-lap shear tests.

The static tensile tests were carried out under quasi-static conditions according to the standard ASTM D638 both for the definition of the geometry of the samples (Type I in this case) and the specifications for the test in terms of crosshead speed, set at 50 mm/min. Please refer to Fig. 3 and Table 3 for the details. The tests were performed using the 100 kN MTS Insight electromechanical universal testing machine at room temperature. For each material, at least 5 repetitions were carried out. The mechanical

**Table 2** DSC parameters for the thermal characterization

Material	Temperature interval, °C	Reference	Melting enthalpy, J/g	Reference
PP	20–200	[32, 33]	207	[34]
PA66	20–300	[35, 36]	226	

**Fig. 2** Typical TGA/DTG diagram for the evaluation of the degradation characteristics



properties here investigated were the Young’s modulus ( $E$ , GPa), the ultimate tensile strength ( $UTS$ , MPa), the strength at break ( $\sigma_R$ , MPa), the yield strength ( $\sigma_y$ , MPa), and the elongation at break ( $\epsilon_R$ , %). These values were estimated by using the MATLAB® software.

After the laser irradiation, the percentage variation of the tensile properties ( $\Delta\%$ ) compared to the untreated polymers were calculated according to Eq. (2), where  $x_T$  is the property after the treatment, while  $x_U$  is the property of the original material:

$$\Delta\% = \frac{x_T - x_U}{x_U} 100 \tag{2}$$

Then, after joining the polymers with the metal substrate, the strength of the hybrid joints was evaluated through single-lap shear tests through the use of the MTS Insight 322 electromechanical universal testing machine, equipped with a 50 kN load cell. The tests were carried out under quasi-static conditions with a constant cross-head speed of 1.27 mm/min at room temperature. These

test specifications, as well as the sample geometry (shown in Fig. 4), were defined according to the standard ASTM D3163.

The test allowed the evaluation of the shear strength ( $\tau$ , MPa), defined as the ratio between the ultimate shear force ( $USF$ , N) and the section of the joined area ( $A$ , mm<sup>2</sup>). It is worth noting that  $A$  varies for each sample and it was estimated through the analysis of the fracture surfaces by using the software ImageJ. The images were captured with the high-resolution digital camera Canon D60 equipped with the 100F28 macro lens. Figure 5 shows an example on the methodology here adopted: the area of interest is identified through the polygonal selection operation and then measured on both sides of the joints, if applicable. This is necessary because, if the polymer flows into the

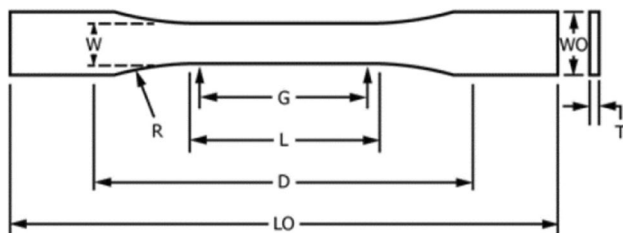


**Fig. 3** Type I sample geometry according to the standard ASTM D638 for static tensile test

**Table 3** Geometric parameters and specifications for tensile tests according to standard ASTM D638

Parameter	Value	Unit
Thickness ( $T$ )	< 7	mm
Length ( $L$ )	57	mm
Width ( $W$ )	13	mm
Overall length ( $LO$ )	165	mm
Overall width ( $WO$ )	19	mm
Gage length ( $G$ )	50	mm
Clamps distance ( $D$ )	115	mm
Fillet radius ( $R$ )	76	mm
Crosshead speed <sup>i</sup>	5      50      500	mm/min

The more rigid the material, the lower the crosshead speed. In this study, a crosshead speed of 50 mm/min was adopted

<sup>i</sup>The choice is based on the rigidity of the material

**Fig. 4** Sample geometry according to the standard ASTM D3163 for single-lap shear test

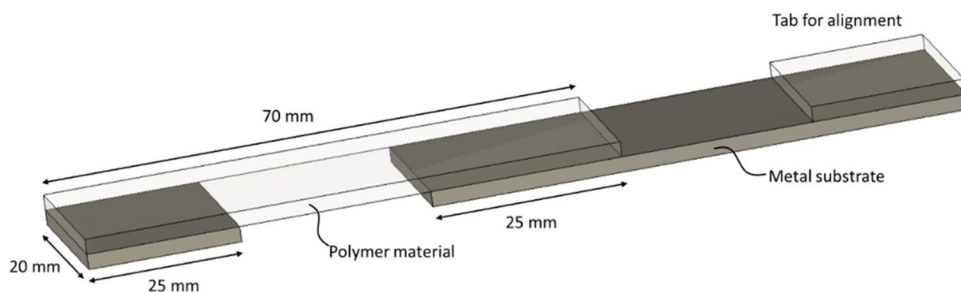
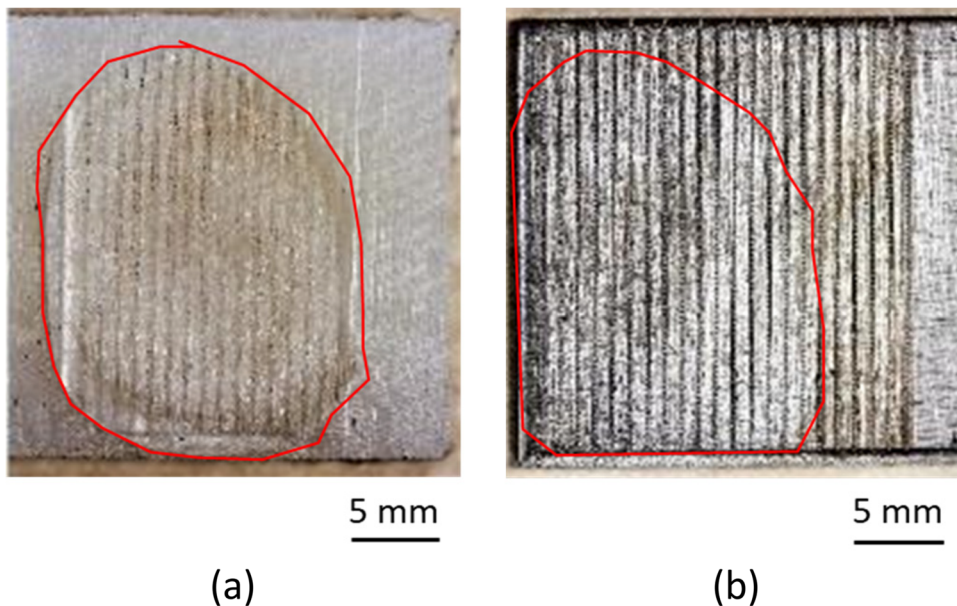


**Fig. 5** Polygon selection of the joint area after the shear testing: polymer side (a) and metal side (b)



texture of the metal substrate during the laser irradiation, it can lead to a smaller residual joint area. The polygonal selection therefore takes place by excluding any residual polymer solidified on the metal substrate outside the maximum area analyzed. Moreover, the morphology of the obtained joints after testing were analyzed through the inspection of the transverse cross section by using the digital microscope KH-8700 by Hirox. The samples were cut near the central section by means of an abrasive cutting blade and prepared according to the relevant standard procedures for the preparation of metallographic samples.

## 2.5 Laser treatment

Laser treatments on the materials here adopted, both polymeric and metallic, as well as for the joining process, were carried out by adopting the same system with two different laser sources, i.e. a near infrared diode laser IPG DRL 200 by IPG Photonics with a top-hat intensity distribution for the polymers treatment and the joining process, while an infrared fibre laser YLPRA30-1-50-20-20 by IPG Photonics with a gaussian intensity distribution for metal treatment,

whose main characteristics are listed in Table 4. It is worth to highlight here that the diode laser was equipped with a beam expander 5× allowing a laser spot of about 30 mm.

### 2.5.1 Laser-polymer interaction

To properly set the process parameters to be adopted during the joining process, the study of the laser-polymer interaction concerned the definition of the transmitted power through the estimation of the Lambert-Beer law on as-received plates with a smooth surface.

In general, depending on the laser beam energy, material thickness, and material crystalline structure, a different

**Table 4** Main characteristics of the laser sources

Characteristic	Value	
	<i>IPG DRL 200</i>	<i>YLPRA30-1-50-20-20</i>
Wavelength, nm	975	1064
Nominal power, W	200	30 (average)
Spot diameter, mm	6	0.09

absorption is expected [39]. Therefore, to define the distribution of heat inside the polymer materials, the Lambert-Beer absorption law was considered. This is of particular interest as it allows determining the transmitted rate, which is a crucial factor during the joining operation. So, the laser treatment of polymer materials concerned the estimation of the transmitted laser energy by measuring the laser power detected with and without the polymer according to the setup schematized in Fig. 6. For each test, the irradiation time was set at 10 s, while the power was varied between 10 and 50% of the nominal value 200 W with steps of 10%. During the tests, the surface temperature of the polymer samples was acquired using the infrared thermal camera A665sc by FLIR, while the transmitted power with the OPHIRF150A-SH sensor connected to the Nova Display Assy power metre by OPHIR. During each irradiation test, 3 measurements of the transmitted power were acquired, calculating then the mean value. The samples consisted of plates 25 mm in width and 70 mm in length.

The Lambert-Beer law is a relationship that correlates the quantity of radiation absorbed by a material to the thickness of the material itself and hypothesizes exponential absorption of radiation as the thickness ( $x$ ) varies: when a beam of light (monochromatic) passes through a medium with an initial intensity  $I_0$ , part is absorbed by the medium and part is transmitted with residual intensity  $I$ , which are related by the attenuation coefficient  $k$  according to Eq. (3):

$$I = I_0 e^{-kx} \quad (3)$$

This law allows to determine the transmitted laser power as the thickness of the polymer varies. However, the so-defined transmission coefficients are valid only for the thickness tested during the experiments. In general, in fact, if the thickness varies, the transmission coefficient varies as well, since the length of the path that the radiation must go through changes. Therefore, to experimentally determine the absorption law through regression analysis, it is essential to use samples of different thickness. In this case, since the

starting slabs have a single thickness for each type of polymer, the proposed solution is to use multi-layered samples by coupling two or more of them together. These, if well-cleaned and well-matched by the application of a coupling force between the layers, to avoid or limit any internal radiation reflection, will behave, with good approximation, as a single sample with double thickness or more [40]. Figure 7 shows the schematization of the experimental setup with a single layer compared to the multi-layered ones consisting of one up to a maximum of four layers. For each test, the irradiation time was set at 10 s, while the power was varied between 50 and 100 W.

When the laser beam hits the polymer plate, the radiation can be reflected, absorbed, and/or transmitted. In general, for the conservation of energy, the hitting laser power ( $P_L$ ) can be written as the sum of the three mentioned contributions, i.e. reflected power ( $P_R$ ), absorbed power ( $P_A$ ), and transmitted power ( $P_T$ ), as described by Eq. (4):

$$P_L = P_R + P_A + P_T \quad (4)$$

The terms  $P_L$  and  $P_T$  can be experimentally estimated by adopting the setups schematized in Fig. 7, while  $P_R$  can be calculated by the Lambert-Beer law considering the thickness  $x$  in Eq. (3) equal to zero, i.e. corresponding to an infinitesimal penetration of radiation into the material, so that the residual power inside the first layer of material ( $P_0$ ) equals the incident one ( $P_L$ ) minus the power lost through reflection ( $P_R$ ):

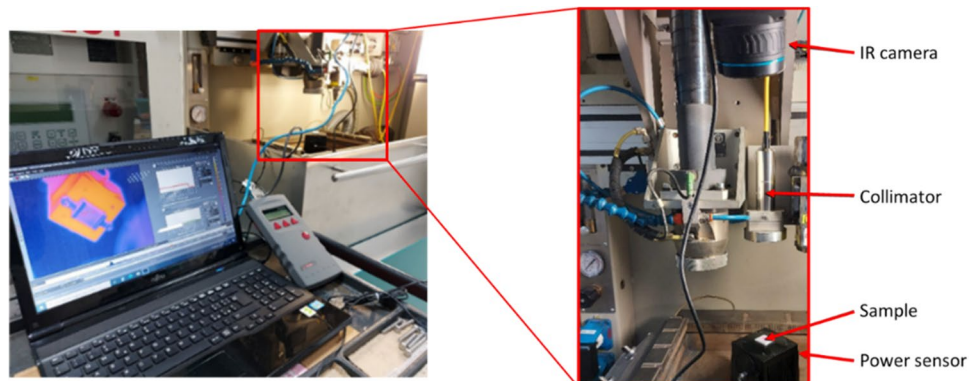
$$P_R = P_L - P_0 \quad (5)$$

Finally,  $P_A$  can be calculated according to Eq. (4).

## 2.5.2 Laser-metal interaction

The study of the interaction between the laser and the metal substrate is important in order to avoid the establishment of any degradation phenomena of the polymer during the joining process. In other words, the surface temperature

**Fig. 6** Experimental setup for the evaluation of the Lambert-Beer law



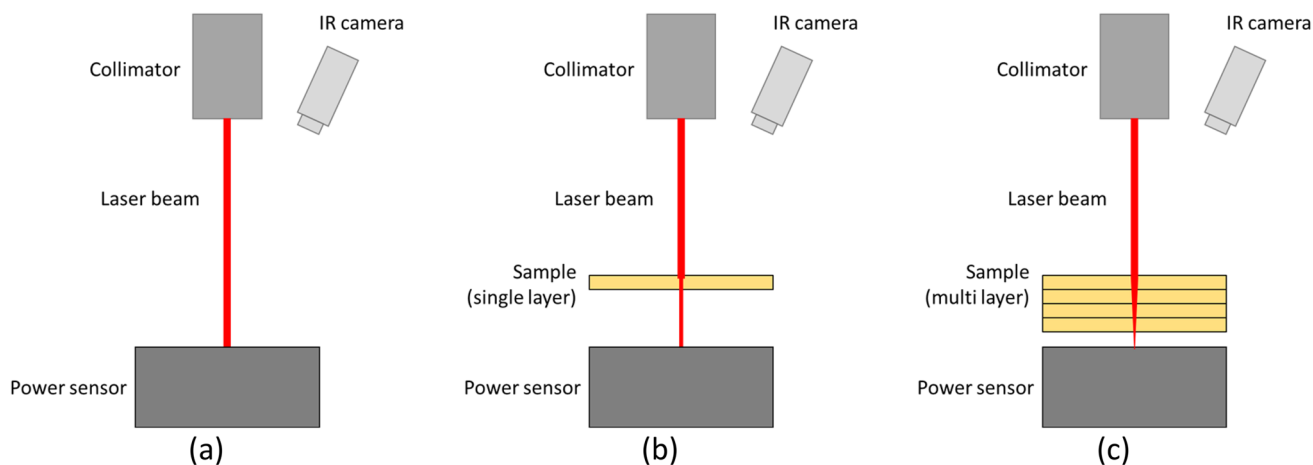


**Fig. 7** Setup schematization for the evaluation of the transmitted laser power without any sample (a), with a single layer (b) and with multi-layered samples (c)

reached on the metal substrate at the interface with the polymer should be higher than the melting point, but lower than the onset temperature of the polymer itself. To this end, the IR camera was used to measure the metal surface temperature during the interaction with the laser at varying set laser power (i.e., 100 W, 150 W, and 200 W) and processing time (i.e. up to 210 s). So, to determine the suitable process time-temperature range, the melting and degradation temperatures of the polymer materials, as well as the amount of transmitted energy during the laser-polymer interaction, were taken into consideration.

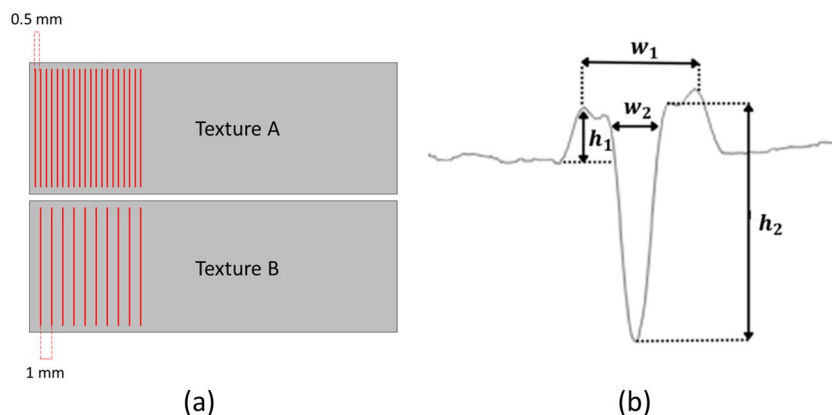
Moreover, in addition to the set laser power and processing time, a third factor, here considered for the definition of the experimental plan to be adopted during the joining process, was the surface texture of the metal substrate. In fact, since polymers and metals are commonly characterized by a poor surface chemical affinity [20], the texture is aimed at promoting the mechanical bonding between the two different materials through the interlocking mechanism [41]. Two types of texture were obtained by using the diode laser by setting the following process conditions: average

power of 30 W, pulse repetition rate of 30 kHz, scanning speed of 2000 mm/s, and with 30 repetitions for each path. It is worth noting that such values were chosen according to preliminary tests here not reported for sake of brevity. The textures consisted in consecutive scan lines spaced respectively of 0.5 mm and 1 mm (Fig. 8a). Finally, after cleaning the textured surfaces by using an ultrasonic bath in water (for an immersion time of 10 min) to remove any residues, the textures were observed and characterized by means of the digital microscope KH-8700 by Hirox equipped with a 2.11 MP CCD sensor. The estimated parameters were the width of the profile considering the metal burr ( $w_1$ ), the kerf width ( $w_2$ ), the burr height ( $h_1$ ), and the kerf height ( $h_2$ ), as shown in Fig. 8b. Moreover, the arithmetical mean roughness ( $Ra$ ) and the mean roughness depth ( $Rz$ ) were also determined.

### 2.5.3 Laser-assisted joining

The experimental joining setup was properly designed to ensure the contact between the materials' surfaces during laser irradiation. Specifically, the gripping system was

**Fig. 8** Textures schematization (a) and their characterization (b). Width of the profile considering the metal burr ( $w_1$ ), kerf width ( $w_2$ ), burr height ( $h_1$ ), kerf height ( $h_2$ )





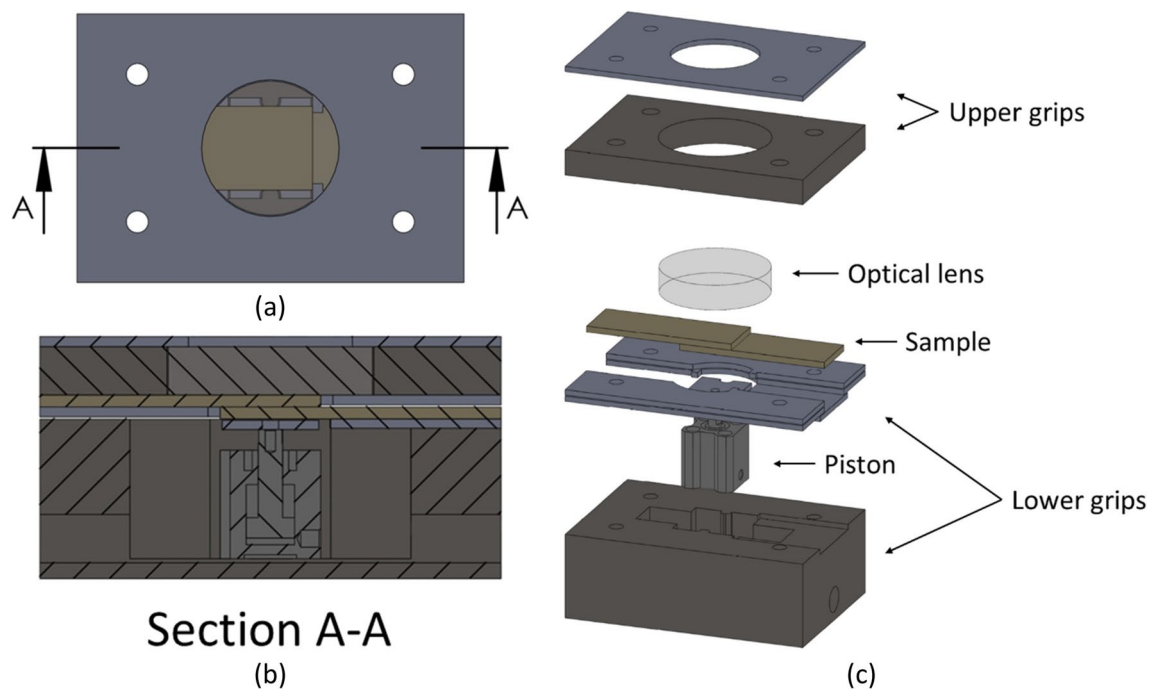


**Fig. 9** Setup schematization of the gripping system for the joining process: **a** top view, **b** section view, and **c** exploded view

aimed to apply a clamping pressure of approximately 1.0 MPa. Figure 9 shows the schematization of the system and its exploded view. As can be seen in the latter, it consists of two grips clamped together, and by means of a piston, the pressure is applied to the centre of the sample at the overlapping through compressed air. Since the polymers here considered are transparent to the wavelength of the laser adopted, they were positioned on the top side where the laser beam comes from. This will pass through the polymer, heating the metal substrate below, and the joining will take place through thermal conduction. Figure 10 shows a schematization of the process and the resulting setup adopted for the laser-assisted joining. The irradiated area of the sample (highlighted in pink in the latter figure) covers a surface of

550 mm<sup>2</sup> over 625 mm<sup>2</sup> available from the overlapping of the samples.

The experimental plan was designed using the Design of Experiment methodology using Minitab 18 software. The full factorial experimental plan with 3 factors (i.e., set laser power, interaction time, and texture of the metal substrate) and 2 levels of control for each of them was considered, as detailed in Table 5. A total of 8 different combinations was replicated 3 times for a total of 24 specimens made for each material combination (i.e. PP/SS304 and PA66/SS304). It is worth noting that the interaction time and the set laser power levels to adopt for the experiments were established on the basis of the results obtained during the study of the laser-polymer interaction and the findings of the thermal

**Fig. 10** Setup schematization of the polymer-metal positioning (**a**) and final setup (**b**). The pink zone represents the irradiated area with an extent of 550 mm<sup>2</sup>

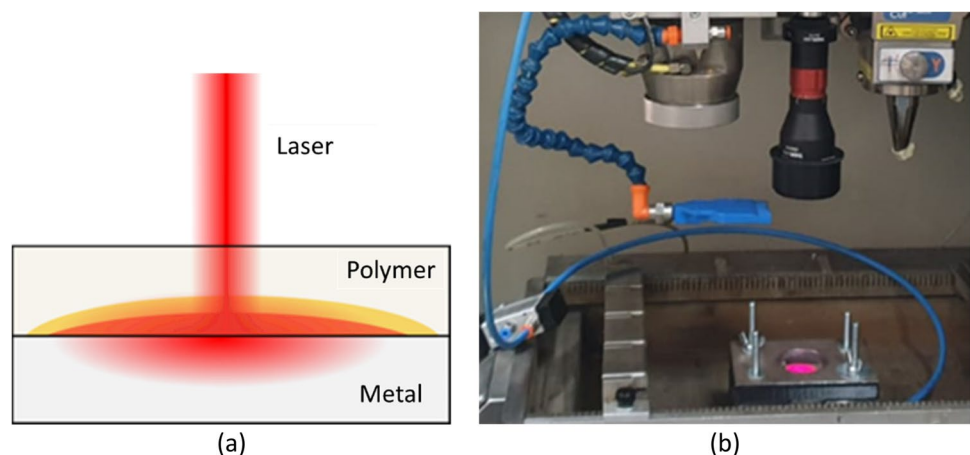


**Table 5** Process parameters and their levels for the definition of the experimental plan. 2 levels of set laser power  $\times$  2 levels of interaction time  $\times$  2 levels of metal surface texture  $\times$  3 replications = 24 tests for each material

Parameter	Level			
	PP		PA66	
Set laser power, W	150	200	150	200
Interaction time, s	30	50	80	100
Metal surface texture <sup>1</sup>	A	B	A	B

<sup>1</sup>Texture A is represented by scan lines spaced 0.5 mm each other, while texture B spaced 1 mm (see Fig. 8a)

characterization tests carried out on the polymers, considering the relative melting and degradation temperatures, while the textures A and B on the metal surfaces are obtained with parallel scan lines spaced, respectively, 0.5 mm and 1 mm.

After the joining process, the samples were tested according to the procedure presented in Section 2.4. Finally, the results were analyzed through the ANOVA statistical method by using the software Minitab version 18. The analysis was carried out with a confidence level of 95%, i.e.  $p$ -value lower than 0.05. To further confirm the significance of the influence of the process parameters on the response variables, the Fisher value ( $F$ -value) was evaluated. If the  $F$ -value is greater than the tabulated one [42], i.e.  $F$ -critical, then the effect can be considered significant. For this study, the  $F$ -critical were 4.67 for PP/SS304 and 4.54 for PA66/SS304 considering, respectively, 14 and 15 observations and 1 degree of freedom for each control factor.

### 3 Results and discussion

According to the flowchart showed in Fig. 1, this research study concerned three main activities: (i) the first one was aimed at defining the fundamental mechanical and thermal properties of the polymers, i.e. PP and PA66, to properly tune the laser processing parameters for irradiation; (ii) then, the interaction mechanisms between the laser and the materials, as well as any modification in the mechanical and thermal properties induced by the treatment, were investigated; (iii) finally, after the realization of the experimental setup to join the materials, and according to the experimental plans properly developed, the produced hybrid joints were tested and inspected. The details are in the following sections.

#### 3.1 Polymers' treatment

The preliminary characterization of polymers was carried out through static tensile tests for the evaluation of the mechanical properties, and through DSC and TGA to

investigate the degradation properties. Then, to correctly set the laser process parameters to be adopted during the joining process, the polymers were treated by using the IR diode laser while varying the set laser power and the material thickness (for increasing layers' number from 0 to 4). The setup presented in Section 2.5.1 allowed to directly measure the laser power that passes through the polymer (transmitted power) and simultaneously monitor the surface temperature of the polymer samples by using the IR camera. So, the tensile test and the DSC were performed again on the treated samples to evaluate any change induced by the laser processing.

##### 3.1.1 Thermal characterization

The DSC tests were carried out by setting the temperature range between 20 and 200 °C for PP [32, 33] and between 20 and 300 °C for PA66 [35, 36]. The quantity of material used was 6.3 mg and 6.4 mg for PP and PA66, respectively. Table 6 collects the properties of main interest, i.e. melting temperature ( $T_m$ , °C), crystallization temperature ( $T_c$ , °C), glass transition temperature ( $T_g$ , °C), and degree of crystallinity ( $X_c$ , %). For both materials, the table suggests that after the first cycle of heating/cooling, the melting point is lower. This is due to the structural reorganization of the polymer molecules that are not able to crystallize in the same amount as they were originally. This is supported by the change in the degree of crystallinity, which is reduced from 41.49 to 38.62% for PP and from 26.45 to 24.44% for PA66. Moreover, PA66 shows a glass transition around 55 °C, which remains almost unchanged during the second cycle, while two melting points can be observed, which are typical of the phase transition from  $\alpha$  to  $\gamma$  of the crystalline structure of nylon [43]. These aspects are of crucial importance because a change of the crystalline structure can severely affect the mechanical properties of the polymer itself. Moreover, the TGA tests allowed the determination of the degradation properties, i.e. the first derivative temperature ( $T_{DTG}$ , °C), the extrapolated onset temperature ( $T_{on,E}$ ,

**Table 6** Thermal properties and degree of crystallinity of polymers before laser irradiation

Property	PP		PA66		
	Cycle I	Cycle II	Cycle I	Cycle II	
$T_m$ , °C	168.20	167.98	261.75	250.29	258.89
$T_c$ , °C	112.04	112.46	226.74	225.02	
$T_g$ , °C	-	-	55.53	55.49	
$X_c$ , %	41.49	38.62	26.45	24.44	
$T_{DTG}$ , °C	458		438		
$T_{on,E}$ , °C	432		419		
$R_m$ , %	0.3		2.9		

**Table 7** Operational parameters for the laser treatment of the polymeric samples

Parameter	PP	PA66
Set laser power, W	200	200
Interaction time, s	300	110
Maximum surface temperature, °C	135	195

°C), and the percentage of material residue ( $R_m$ , %). Despite a higher melting temperature for the PA66 is found during the DSC tests, around 260 °C against 168 °C for PP, the nylon is characterized by a lower onset temperature, around 419 °C against 432 °C for PP. This means that the interval within which perform the laser treatment is narrow, so that to require a more careful tuning of the laser parameters.

To evaluate the properties of the polymers after laser irradiation, the samples were treated by varying the laser power and the duration of the interaction time in order to bring the temperature of the sample close to the melting one (around 75–80%), according to the preliminary investigation (see Table 6). During the treatment, the surface temperature was monitored through the IR camera. Table 7 lists the operational parameters and the maximum surface temperature for both polymers, while Table 8 collects the thermal properties after laser irradiation. As can be seen, there is a slight change of the melting and crystallization temperatures, i.e. lower than 1%, while the degree of crystallinity decreases for both materials, with a more marked effect for PA66, which is around 17% during the first heating cycle, and around 12% during the second one, against a decrease of about 2% for PP. This reduction, for both polymers, could be explained by the formation of radicals during the laser treatment as result of the partial depolymerization they undergo. As a consequence, the fine order of the polymer chains is lost, and the degree of crystallinity decreases [44, 45].

### 3.1.2 Mechanical characterization

The static tensile tests were carried on five samples for each polymer material, i.e. PP and PA66, whose geometry is shown in Fig. 3, by adopting a crosshead speed of 50 mm/min. Table 9 reports the results obtained through the analysis of the stress-strain curves in terms of mean

**Table 8** Thermal properties and degree of crystallinity variation of the treated samples

Property	PP		PA66		
	Cycle I	Cycle II	Cycle I	Cycle II	
$T_m$ , °C	+0.10%	-0.42%	+1.00%	+0.89%	+0.44%
$T_c$ , °C	+0.16%	-0.11%	-0.51%	-0.36%	
$X_c$ , %	-1.16%	-2.33%	-16.82%	-11.99%	

**Table 9** Static tensile test results before (as mean value  $\pm$  standard deviation) and after the laser treatment (as percentage variation)

Property	Before laser treatment		After laser treatment	
	PP	PA66	PP	PA66
$E$ , GPa	$1.79 \pm 0.06$	$1.55 \pm 0.03$	+21.8%	-8.9%
$UTS$ , MPa	$32.29 \pm 0.31$	$53.70 \pm 1.00$	+1.5%	+1.1%
$\sigma_R$ , MPa	$22.00 \pm 0.334$	$40.48 \pm 2.44$	+5.0%	-4.6%
$\sigma_y$ , MPa	$15.42 \pm 1.75$	$12.59 \pm 1.39$	-14.0%	-17.1%
$\epsilon_R$ , %	$88.85 \pm 9.77$	$54.94 \pm 2.24$	-66.3%	-28.6%

values  $\pm$  standard deviation before and after the laser irradiation, while Fig. 11 shows the samples after the tensile test. As can be seen, for both polymers, there is a variation of the mechanical properties induced by the treatment. The most influenced parameter is the elongation at break, with a decrease of 66.3% for PP and 28.6% for PA66. In fact, as shown in Fig. 11, during the tensile test, the narrowing forms in two different zones, i.e. above and below the irradiated area, and the breakage of the specimens occurs preferentially at one of them, therefore outside the treated area. Based on this, it can be deduced that the material has not experienced a degradation of the mechanical properties at the irradiated area. However, due to the laser treatment, the samples undergo to an annealing treatment which may vary the crystal structure [46],

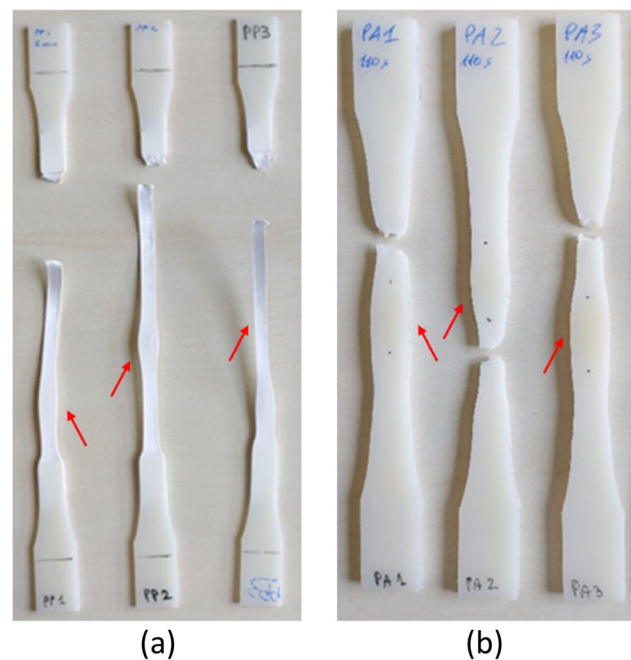


**Fig. 11** Irradiated tensile specimens after testing: PP (a) and PA66 (b). The red arrows indicate the irradiated area during the laser treatment

**Table 10** Transmitted power measurements for one layer of smooth material. The incident power refers to the measured value of laser power without any material along the path

Set power, W	Measured power, W			Maximum surface temperature, °C	
	Incident	PP	PA66	PP	PA66
20	13.2	6.3	3.1	32.8	39.1
40	39.9	18.9	9.4	81.7	52.4
60	65.2	30.0	16.3	64.9	75.8
80	90.5	39.6	23.1	97.5	81.0
100	114.5	48.0	29.7	138.3	160.0

and the degree of crystallinity is reduced. Therefore, the volume of the amorphous phase is increased, while there is a confinement of the crystallites around the amorphous chains which affects chain mobility through a decreasing in the entanglements and therefore resulting in a reduced elongation [47].

### 3.1.3 Energy partition

During the laser joining process, the phenomenon of absorption and transmission of light radiation through the thickness of the polymer to the metal surface is of crucial importance since they control the propagation and transfer of energy as heat [39, 48], which can eventually lead to material melting or vaporization necessary for the realization of the joint [49]. Moreover, rough surfaces could lead to a decrease in the amount of both absorbed and transmitted power contributions, which can be detrimental for the success of the joining process itself [50, 51], while the laser energy absorption and transmission can be maximized by irradiating a smoother surface, which is supposed to offer an improved strength when joined with metals [52]. In this context, Table 10 and Fig. 12a show the preliminary results for one layer, while Fig. 12b and Table 11 for increasing layers, for the as-available smooth polymers. Figure 12a suggests a good linearity between the transmitted and the incident power values, meaning that the irradiated materials do not undergo damage during the treatment. This is also supported by the maximum values of the surface temperature, collected in Table 10, that remain lower than the degradation conditions

**Fig. 12** Transmitted power measurements for one layer (a) and increasing number of layers (b) of smooth polymers. The thickness of the single layers is 3.04 mm for PP and 5.76 mm for PA66

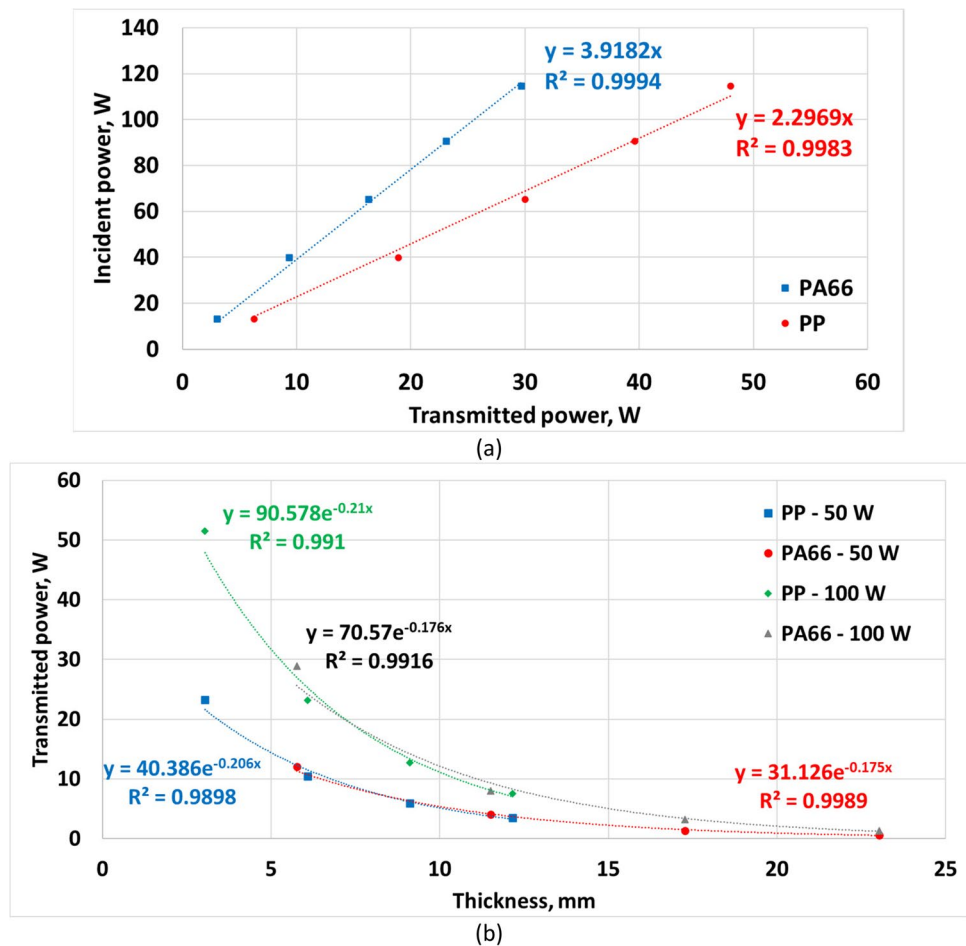


**Table 11** Resulting partitions of power for increasing layers of as-received smooth material

Material	$P_L$ , W	$P_0$ , %	$P_R$ , %	Layers	Thickness, mm	$P_T$ , %	$P_A$ , %
PP	50	80.77	19.23	1	3.04	46.50	34.27
				2	6.08	21.00	59.77
				3	9.12	11.86	68.91
				4	12.16	6.96	73.81
	100	83.87	16.13	1	3.04	47.69	36.18
				2	6.08	21.48	62.39
				3	9.12	11.80	72.07
				4	12.16	6.94	76.92
PA66	50	62.45	37.55	1	5.76	24.01	38.44
				2	11.52	8.05	54.40
				3	17.28	2.66	59.79
				4	23.04	1.19	61.26
	100	65.32	34.68	1	5.76	26.76	38.56
				2	11.52	7.39	57.93
				3	17.28	2.95	62.37
				4	23.04	1.24	64.08

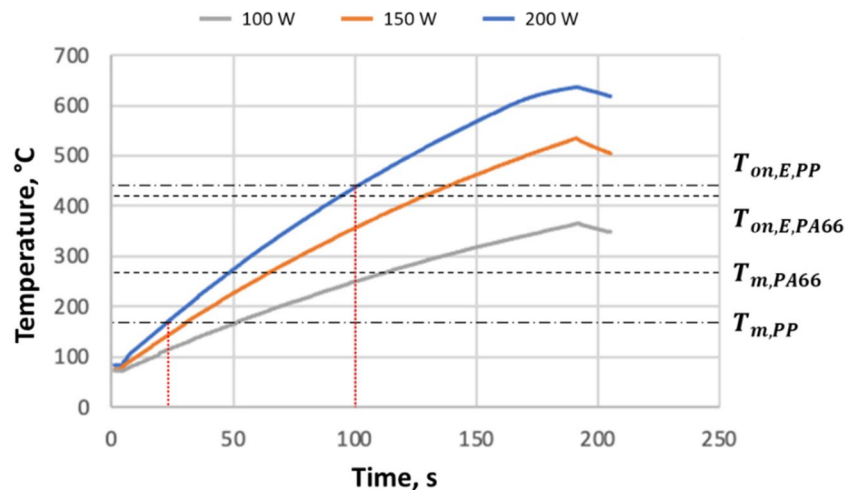
identified through TGA, i.e. 138.3 °C against 432 °C for PP and 160.0 °C against 419 °C for PA66. However, it is worth noting that these findings are valid for the specific materials, under the experimental conditions here adopted, i.e. irradiation time of 10 s and laser wavelength of 975 nm, and only for the thickness tested, i.e. 3.04 mm for one layer of PP and 5.76 mm for one layer of PA66. A greater thickness implies a longer path that the radiation must pass through to move from the upper face to the lower one, and therefore, a greater absorption is expected. This is factually confirmed by the laser treatments carried out for varying layer numbers, as shown in Fig. 12b. It is worth noting from the latter figure that the equations, obtained with the exponential regression of the experimental data, represent with a very good approximation the Lambert-Beer law described by Eq. (3), i.e.  $R^2 \approx 1$ . Moreover, the difference between the attenuation coefficients  $k$  for the two measurements at 50 W

and 100 W of hitting laser power ( $P_L$ ) for both materials is negligible, i.e. lower than 2% for PP and lower than 0.6% for PA66. Finally, Eqs. (4) and (5) were applied according to the procedure described in Section 2.5.1 to evaluate the partitions of power among transmission ( $P_T$ ), absorption ( $P_A$ ), and reflection ( $P_R$ ), as detailed in Table 11.

### 3.2 Metal treatment

The suitable process time-temperature range within which carry out the joining process was evaluated by irradiating the metal substrates while recording the surface temperature and duration time. Figure 13 shows the curves obtained for increasing values of set laser power, i.e. 100 W, 150 W, and 200 W. As can be seen, the optimal range, highlighted by the red dashed lines, is between 25 and 100 s. Within this interval, the maximum temperatures reached on the surface

**Fig. 13** Laser-metal treatment for varying laser power and duration time. The optimal range is highlighted by the red dashed lines (from 25 to 100 s)



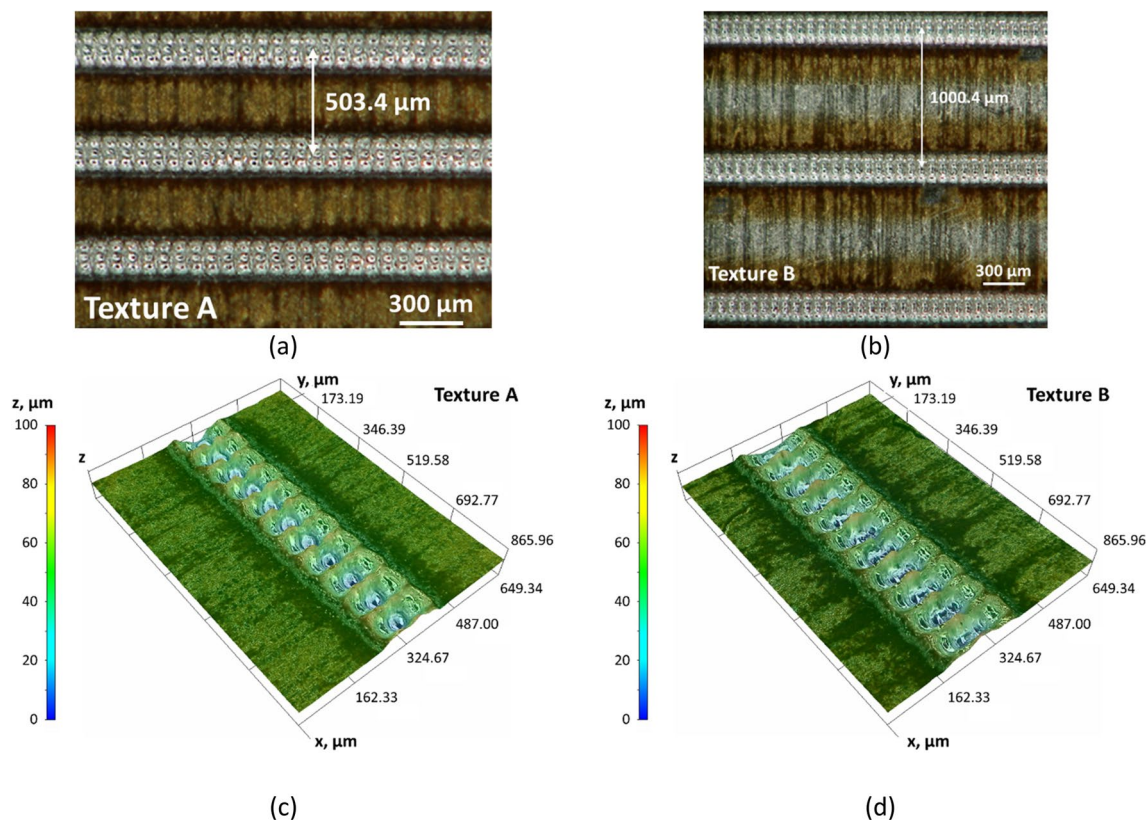


Fig. 14 Irradiated SS304 surfaces for pattern type A (a, c) and B (b, d)

of the metal substrate vary between the melting and the onset temperatures of the PP, i.e. 168 °C and 432 °C. It is worth noting that for the experimental plan to be adopted for the joining process, only two values of laser power were chosen, i.e. 150 W and 200 W, since at 100 W, the time required to reach the melting temperature is long for both polymers. The interaction time was therefore set at 30 s and 50 s for PP and at 80 s and 100 s for PA66. In addition to these two parameters, two types of texture were obtained by using the diode laser setting the average power at 30 W, the pulse repetition rate at 30 kHz, the laser scanning speed at 2000 mm/s, and with 30 repetitions for each path. Figure 14 and Table 12 show the optical images of the textures and the estimated topographical parameters.

### 3.3 Laser-assisted joining

The joining process has been carried out with the experimental setup described in Section 2.5.3 following the full

factorial experimental plan obtained varying 3 factors, i.e. set laser power, interaction time, and texture of the metal substrate, between 2 levels of control for each of them, as detailed in Table 5, for a total of 8 different experimental conditions. Each of this was replicated 3 times for a total of 24 specimens. Figure 15 shows 8 random samples for each combination for both materials. As can be seen, the metal substrate has been numbered to trace the parameter combination. Moreover, it appears clear that for some of the conditions, the application of the pressure through the clamping system, due to the melting of the polymeric material, let it flow outside the overlapping surface with the SS304 substrate.

Figure 16 shows the results of the single-lap shear tests of the hybrid joints in terms of load-displacement curves. As can be seen, the shear test graphs allow to sort the control factors, i.e. set laser power, interaction time, and texture of metal substrate, based on their effect on the resulting shear properties: the texture is the most influencing parameter,

Table 12 Texturing parameters

Parameter	$w_1, \mu\text{m}$	$w_2, \mu\text{m}$	$h_1, \mu\text{m}$	$h_2, \mu\text{m}$	$Ra, \mu\text{m}$	$Rz, \mu\text{m}$
Texture A	220.96	157.61	33.94	9.59	9.33	25.98
Texture B	257.24	200.92	32.19	7.04	12.07	34.05

**Fig. 15** Joined samples SS304/PP (a) and SS304/PA66 (b)



followed by the laser power, and finally the interaction time. In fact, the texture A, characterized by a smaller distance between two consecutive scan lines (i.e. 0.5 mm against 1 mm of texture B), allows the fused polymer to penetrate in a greater number of grooves, therefore increasing the number of interlocking sites, which contribute to a greater resistance. This can be seen in Fig. 17, which shows the joining areas after the test. Moreover, for increasing laser power, both polymers tend to cover the entire textured surface, also overflowing outside the side due to the applied pressure to guarantee the contact between the surfaces. These effects are

further increased by adopting a longer time of interaction. The only exception is the treatment at 200 W and 80 s for the SS304/PA66 joint, where the larger area of texture B can be explained by a smaller penetration effect of the molten polymer inside the metal grooves, which is responsible for the widening of the observed joint surface.

From the inspection of Fig. 17, it is possible to calculate the actual fracture surfaces areas by using the software ImageJ. These values were then used to calculate the shear strength as the ratio between the ultimate shear force and the joining surface area. Figure 18 collects the obtained results

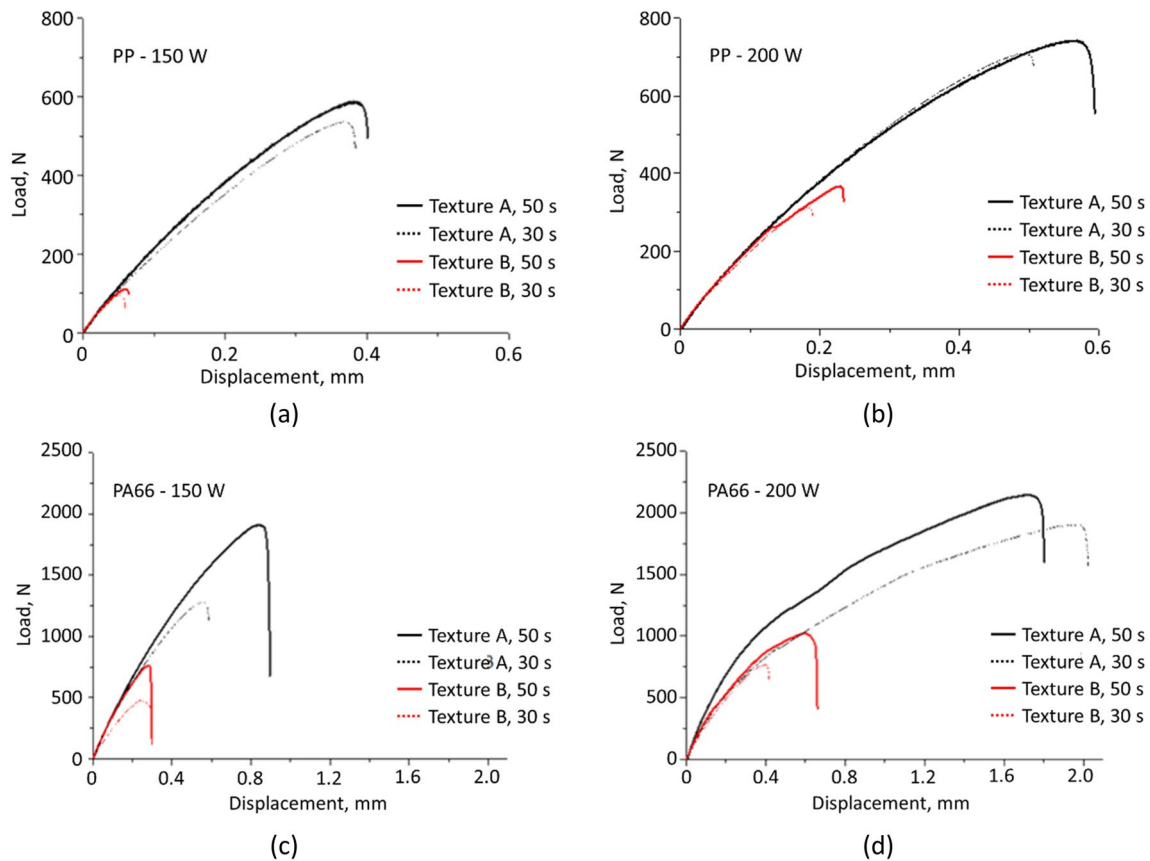
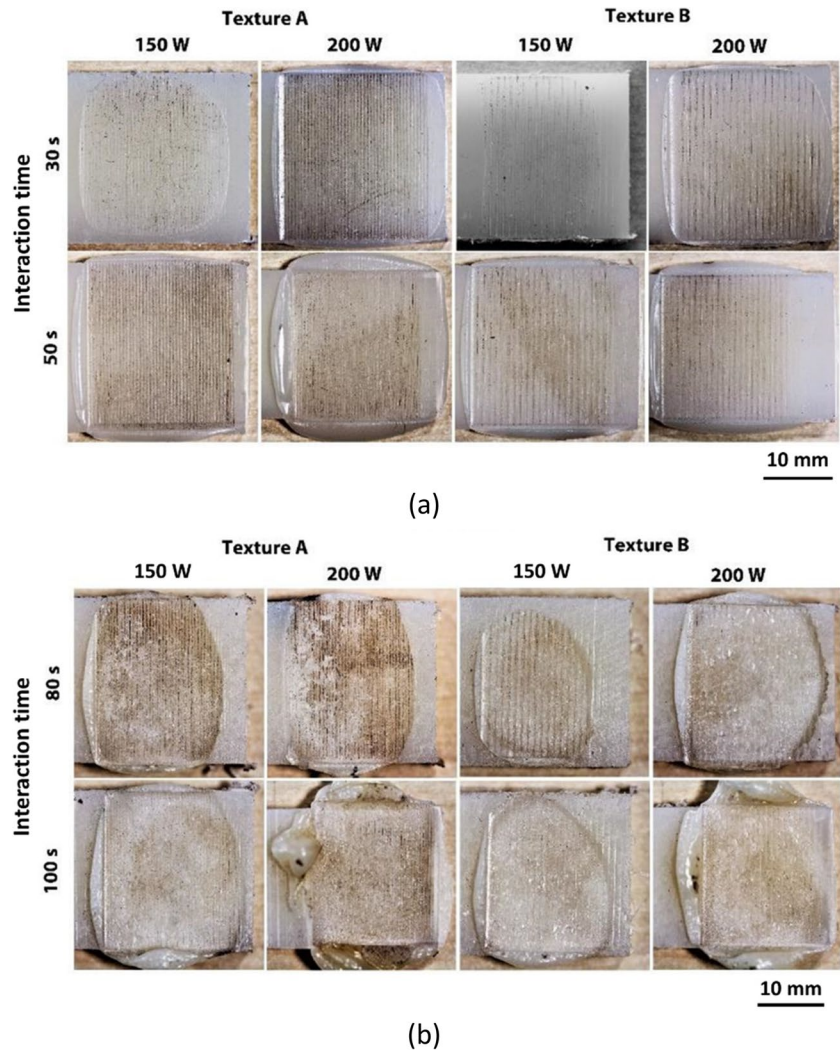


**Fig. 16** Load-displacements curves for SS304/PP (a, b) and SS304/PA66 (c, d) hybrid joints

**Fig. 17** Joining areas after the shear tests for SS304/PP (a) and SS304/PA66 (b)



in terms of ultimate shear force and shear strength. As shown in the latter, according to Fig. 16, the most influencing factor is the surface texture of the metal substrate, with improved *USF* and  $\tau$  for both polymers by using the texture A. Moreover, a proportional improvement of the shear properties can be observed as the interaction time and the laser power increase. Specifically, *USF* reaches a maximum value of approximately 750 N for PP (i.e. around 60% of *UTS*) and 2200 N for PA66 (i.e. around 53% of *UTS*), while the average shear strength reaches ~1.2 MPa for PP and ~3.5 MPa for PA66. This finding can be addressed to the enhancement of the softening of the polymer which is able to better flow inside the grooves and therefore improve the interlocking, considered here the main mechanism responsible for the resistance of the joint [7].

To better understand the influence of process conditions on the shear force of the joints, the fracture surface of the joints on the side of the polymer was further analyzed, since the mechanisms involved during the failure can vary depending on the morphology [10, 53]. Figure 19 shows the fracture

surfaces of the hybrid joints. For SS304/PP (Fig. 19a), the morphology of the textured area indicates that no removal of polymeric material occurred, while for SS304/PA66 (Fig. 19b), the molten polymer mass has moved to a different position compared to the original one, so, especially in the worst joining conditions, i.e. 200 W and 100 s, the structure of the imprinted texture is not clearly visible. In addition to the fracture surface inspection, also the cross sections of the joints were observed, shown in Fig. 20. At the metal-polymer interface, the cavities of textures A and B are visible along the entire sampling length, while the latter figure shows the magnification of some of them to give a better insight of the connections. As previously described, for both combinations of materials, as the laser power and the interaction time increase, the shear force and shear strength increase. In fact, as can be seen in Fig. 20, the mechanism of impregnation of the metal teeth by the polymers was obtained for all the experimental conditions examined. The softening temperatures of both polymers were therefore properly reached, without leading to typical degradation



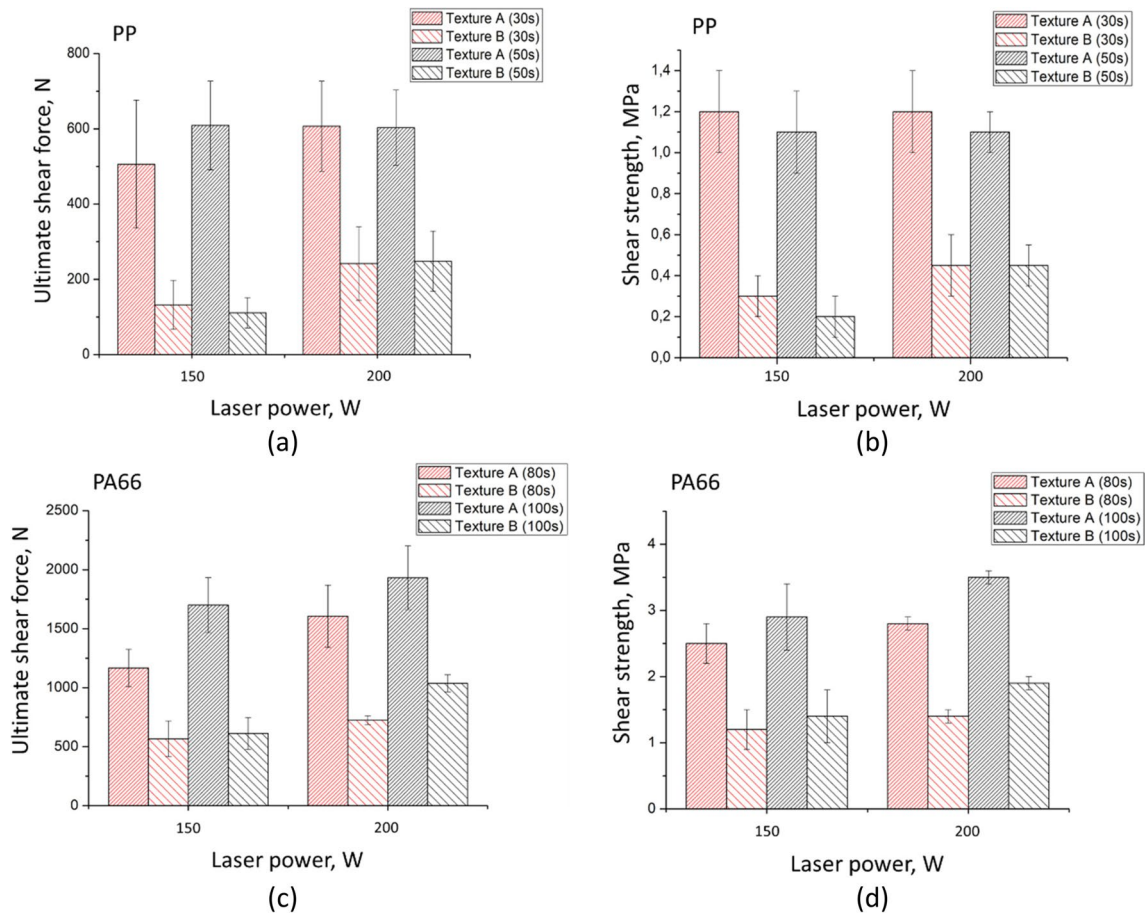


**Fig. 18** Single-lap shear test results for SS304/PP (a, b) and SS304/PA66 (c, d) hybrid joints

phenomena as bubbles or lack of adhesion, except for the most severe treatment for the SS304/PA66 joint at 200 W and 100 s. In this case, the presence of bubbles within the polymer determined the presence of residues of degraded material on large areas of the metal substrate, as shown in Fig. 19b. As a consequence, the fracture surface under these conditions can be considered as a combination of both cohesive and adhesive rupture. However, the resistance of the joints is enhanced. This finding can be attributed to two main coexisting phenomena, i.e. (i) the improved softening of the material which spreads over a larger surface of the metal substrate [25] and (ii) the formation of a greater number of bubbles which can trigger the mechanism of the micro-anchoring through the generated pressure which pushes the molten material within the asperities and therefore improving the joint strength [29, 54]. However, it is worth to note that the voids left by the formation of bubbles at the metal-polymer interface represent vulnerable points where failure can start, thus promoting a premature rupture of the joint.

Finally, the statistical analysis allowed to define any significative influence of the process parameters on the response variables by means of ANOVA tests. The results

consist of a table containing the degrees of freedom ( $DoF$ ), the adjusted sum of squares ( $Adj.SS$ ), the adjusted mean of squares ( $Adj.MS$ ), the  $F$ -value, the  $p$ -value, and the contribution percentage ( $\Pi$ ) of each parameter or parameter combination. Specifically,  $Adj.SS$  provides the variation of each parameter with respect to the response variables, whose contribution is defined through  $\Pi$  as the ratio between  $Adj.SS$  of the analyzed parameter and the total value. The  $F$ -value is used to determine whether a term is associated with the response, comparing the obtained value with the corresponding tabulated one (i.e. the greater the  $F$ -value the greater the influence). In this case, it is defined as the ratio between the  $Adj.MS$  of the response variable and the  $Adj.MS$  of the error. Modelling data using ANOVA methodology requires that four assumptions are verified [55]: (i) the individual observations are mutually independent; (ii) the data fit a statistical model including systematic and random errors; (iii) random errors are normally distributed; and (iv) the variance of random errors is homogeneous. This can be done by means of residual analysis, which is not reported here for sake of brevity, but satisfying the requested requirements. Table 13 and Table 14 show the ANOVA results, in

**Fig. 19** Magnifications of the fracture surfaces after shear test for SS304/PP (a) and SS304/PA66 (b)

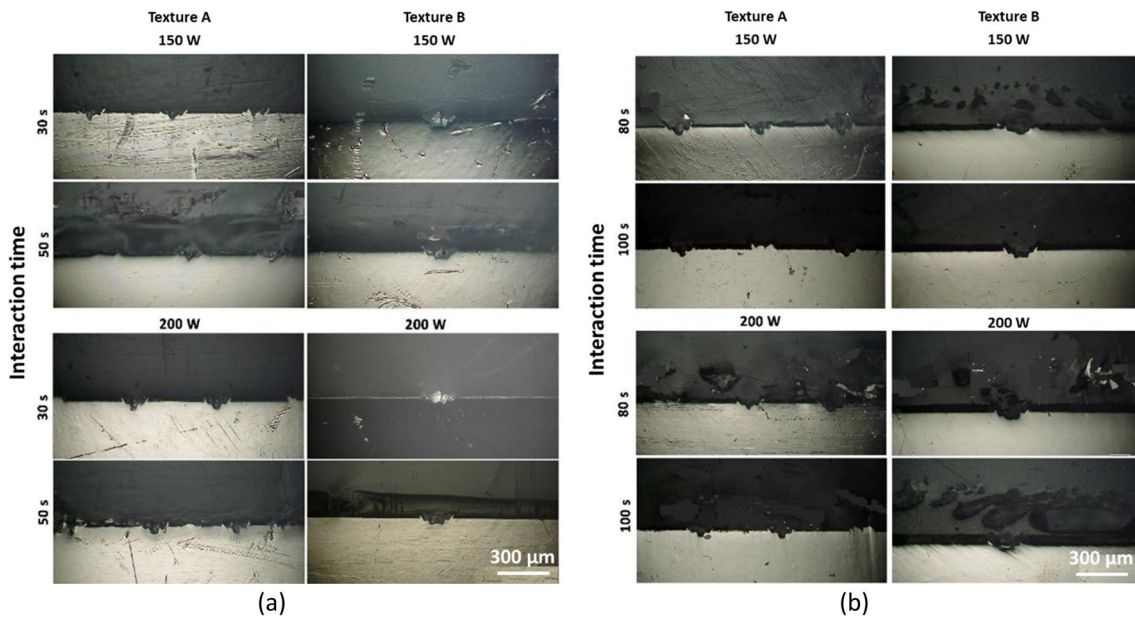
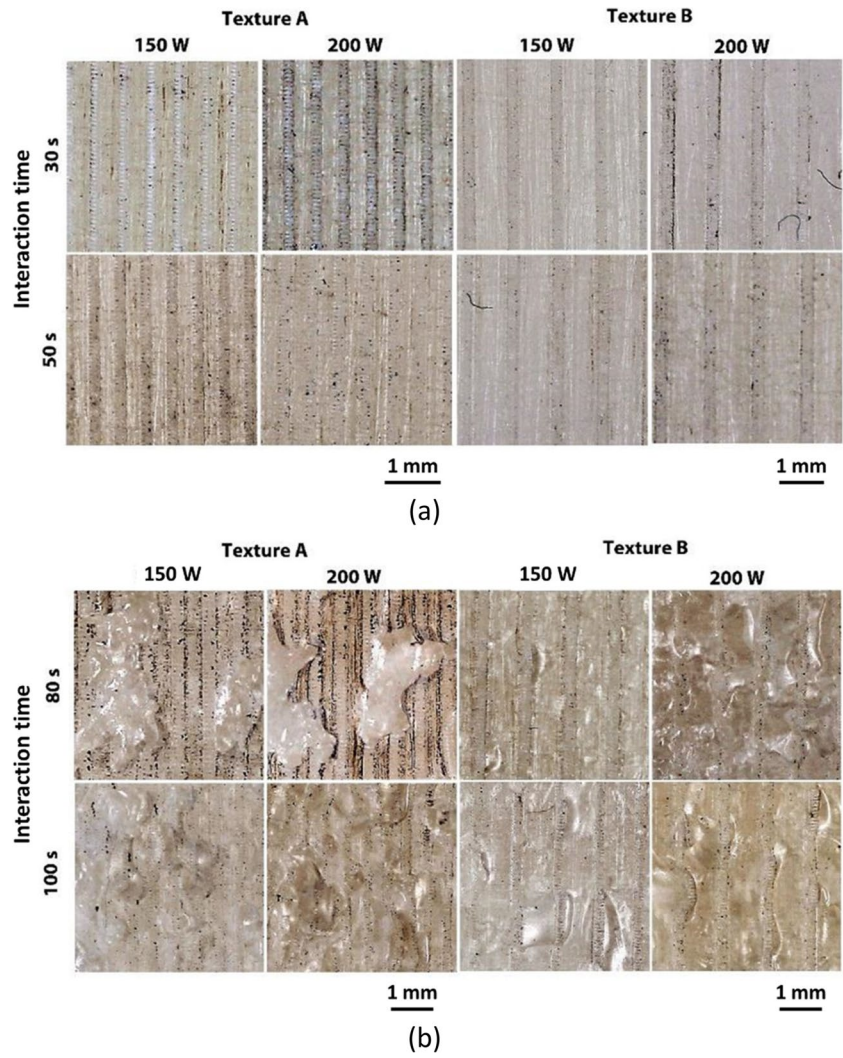


**Fig. 20** Cross sections after the shear test for SS304/PP (a) and SS304/PA66 (b) samples

**Table 13** ANOVA results for the joint SS304/PP. The *F*-critical is 4.67

Source	USF			A			τ		
	<i>F</i> -value	<i>p</i> -value	Π, %	<i>F</i> -value	<i>p</i> -value	Π, %	<i>F</i> -value	<i>p</i> -value	Π, %
Set laser power ( <i>P</i> )	-	-	-	15.68	0.001	16.71	-	-	-
Interaction time ( <i>t</i> )	-	-	-	32.82	0.000	34.99	-	-	-
Texture	24.97	0.000	45.12	-	-	-	22.08	0.000	57.36
<i>P</i> × <i>t</i>	-	-	-	15.68	0.001	16.71	-	-	-

**Table 14** ANOVA results for the joint SS304/PA66. The *F*-critical is 4.54

Source	USF			A			τ		
	<i>F</i> -value	<i>p</i> -value	Π, %	<i>F</i> -value	<i>p</i> -value	Π, %	<i>F</i> -value	<i>p</i> -value	Π, %
Set laser power ( <i>P</i> )	11.67	0.004	11.10	9.05	0.009	24.80	-	-	-
Interaction time ( <i>t</i> )	6.66	0.021	6.34	-	-	-	-	-	-
Texture	64.57	0.000	61.43	-	-	-	19.69	0.001	47.83

which only the *F*-value, the *p*-value, and the Π term of each significant effect (i.e. *F*-value > *F*-critical, *p*-value < 0.05, and Π > 5%) are reported for brevity.

From the statistical analysis it is evident that the texture is the most decisive factor for both hybrid joints, with a contribution percentage greater than 45% and 61% for the ultimate shear force and greater than 57% and 47% for the shear strength for SS304/PP and SS304/PA66 respectively. While the joining surface area is mostly influenced by the laser power and the interaction time. This finding can be attributed to the fact that increasing both power and treatment duration enhance the energy absorption, resulting therefore in a higher temperature. This leads to an improved melting of the polymers, which distribute over a larger surface area of the substrate, contributing to the overall resistance. It is worth noting that for PP, the increase of the joining area, shown in Fig. 17a, results in a slight decrease of the shear strength while the shear force is slightly improved (see Fig. 18a,b). This suggests that the interlocking mechanism, responsible for the resistance, is established on a bigger surface area, but not in a proportional way with the shear force, thus resulting in a reduced shear strength. However, the major effect for these variables is given by the texture, which allow a greater amount of molten material to flow inside the grooves when these are more numerous, i.e., for texture A.

### 4 Conclusions

The research work wants to propose an innovative solution through the use of laser technology for joining of hybrid structures made of semi-transparent polymers and metals without the need of external fasteners or adhesives, thus providing a push towards to the automation and sustainability of production.

The definition of the optimal laser interaction conditions for the formation of the joints and the identification of the technological process windows depending on the materials to be joined have laid the foundations for the creation of resistant joints as valid alternatives to traditional solutions. In fact, the experimental activity has demonstrated the feasibility of laser joining processes of metal-polymer components using a medium-power diode laser. Polypropylene (PP) and Nylon 6,6 (PA66) were successfully joined with AISI 304 stainless steel (SS304). The control parameters were the laser power, i.e. 150 W and 200 W, and the interaction time, i.e. 30 s and 50 s for PP, 80 s and 100 s for PA66. Moreover, the creation of a texture on the surface of the metal substrate served as pre-treatment with the aim of generating a stronger mechanical interlocking mechanism between the metal and the polymer. Two different types of textures were created varying the distance between two consecutive scan lines, i.e. 0.5 mm for texture A and 1 mm for texture B.

The strength of this type of joints depends on several factors, such as the depth of penetration, the extension of the joint area, the degradation of the polymer. After evaluating the thermal and mechanical properties of the polymer materials before and after the laser treatment, aimed to define the processability window, i.e. melting but not degradation, single-lap shear tests were carried out to evaluate the joints' strength for varying experimental conditions to define the optimal one.

From the shear tests, it is evident how the failure frequently occurs at the metal-polymer interface. A proportional improvement of the shear properties is obtained as the interaction time and the laser power increase. Specifically, the shear force reaches a maximum value of approximately 750 N for PP and 2200 N for PA66, which correspond to ~60% and ~53% of the ultimate tensile strength of the polymer as is, while the average shear strength reaches ~1.2 MPa for PP and ~3.5 MPa for PA66. Moreover, although a too

high laser power and a too long interaction time can lead to the formation of bubbles concentrated preferentially at the interface, the shear strength is improved since a greater amount of energy is absorbed, thus improving the softening of the polymer which is able to better flow inside the grooves ensuring the establishment of a stronger interlocking mechanism on a bigger surface.

The main advantage of the solution is the flexibility, which allows for both texturing the metal surface and the subsequent joining with the polymer with the same system. Moreover, the whole process can be easily controlled by directly acting on the operational parameters, thus potentially automatable. The obtained values of shear force compared to the tensile strength needs to be improved to meet the stringent requirements of the modern aerospace and automotive industries. To this end, further investigations are required to define new textures, e.g. net and dimples, and/or materials combinations, e.g. titanium or aluminium as metals and technopolymers, for improved joints.

**Funding** This study was funded through the Programma Operativo Regionale - POR FESR Lazio 2014–2020, Call “Gruppi di Ricerca 2020”, Project A0375 – 2020-36716 “ Laser joining for New hybrid Structures - LIONS” - CUP: E85F21000820005.

**Data availability** Data will be made available on request.

## Declarations

**Competing interests** The authors declare no competing interests.

## References

- Schricker K, Samfaß L, Grätzel M et al (2020) Bonding mechanisms in laser-assisted joining of metal-polymer composites. *J Adv Join Process* 1:100008. <https://doi.org/10.1016/j.jajp.2020.100008>
- Oplinger DW (1998) Mechanical fastening and adhesive bonding. In: *Handbook of composites*. Springer, US, Boston, MA, pp 610–666
- Lambiase F, Scipioni SI, Lee C-J et al (2021) A state-of-the-art review on advanced joining processes for metal-composite and metal-polymer hybrid structures. *Materials* 14:1890. <https://doi.org/10.3390/ma14081890>
- Khosravani MR, Anders D, Weinberg K (2019) Influence of strain rate on fracture behavior of sandwich composite T-joints. <https://doi.org/10.1016/j.euromechsol.2019.103821>
- Amancio-Filho ST, Dos Santos JF (2009) Joining of polymers and polymer-metal hybrid structures: recent developments and trends. *Polym Eng Sci* 49:1461–1476. <https://doi.org/10.1002/PEN.21424>
- Feistauer EE, dos Santos JF, Amancio-Filho ST (2019) A review on direct assembly of through-the-thickness reinforced metal-polymer composite hybrid structures. *Polym Eng Sci* 59:661–674. <https://doi.org/10.1002/pen.25022>
- Lambiase F, Genna S (2017) Laser-assisted direct joining of AISI304 stainless steel with polycarbonate sheets: thermal analysis, mechanical characterization, and bonds morphology. *Opt Laser Technol* 88:205–214. <https://doi.org/10.1016/j.optlastec.2016.09.028>
- Jiao J, Xu J, Jing C et al (2022) Effect of laser micro-texturing on laser joining of carbon fiber reinforced thermosetting composites to TC4 alloy. *Materials* 16(1):270. <https://doi.org/10.3390/MA16010270>
- Huang Y, Meng X, Wang Y et al (2018) Joining of aluminum alloy and polymer via friction stir lap welding. *J Mater Process Technol* 257:148–154. <https://doi.org/10.1016/j.jmatprotec.2018.02.043>
- Lambiase F, Paoletti A, Grossi V, Genna S (2017) Improving energy efficiency in friction assisted joining of metals and polymers. *J Mater Process Technol* 250:379–389. <https://doi.org/10.1016/j.jmatprotec.2017.08.005>
- Yeh R-Y, Hsu R-Q (2015) Development of ultrasonic direct joining of thermoplastic to laser structured metal. *Int J Adhesion Adhesives* 65:28–32. <https://doi.org/10.1016/j.ijadhadh.2015.11.001>
- Li H, Chen C, Yi R et al (2022) Ultrasonic welding of fiber-reinforced thermoplastic composites: a review. *The Int J Adv Manuf Technol* 120:29–57. <https://doi.org/10.1007/S00170-022-08753-9>
- Zhao S, Kimura F, Kadoya S, Kajihara Y (2019) Experimental analysis on mechanical interlocking of metal-polymer direct joining. *Precision Eng* 61:120–125. <https://doi.org/10.1016/j.precisioneng.2019.10.009>
- Kajihara Y, Tamura Y, Kimura F et al (2018) Joining strength dependence on molding conditions and surface textures in blast-assisted metal-polymer direct joining. *CIRP Ann* 67(1):591–594. <https://doi.org/10.1016/j.cirp.2018.04.112>
- Genna S, Lambiase F, Ponticelli GS (2020) Fuzzy decision-making in laser-assisted joining of polymer-metal hybrid structures. *Int J Adv Manuf Technol* 108:61–72. <https://doi.org/10.1007/s00170-020-05379-7>
- Yusof F, Jamaludin F, Abd Shukor M (2012) A brief review: laser joining of polymer-metal structures. *ASEAN Eng J Part A* 2:5–12. <https://doi.org/10.11113/AEJ.V2.15345s>
- Wang M, Zeng X, Tang X et al (2016) Femtosecond laser direct writing of microholes on roughened ZnO for output power enhancement of InGaN light-emitting diodes. *Optics Lett* 41(15):3463–3466. <https://doi.org/10.1364/OL.41.003463>
- Wang M, Wang H, Li W et al (2019) Defect passivation using ultrathin PTAA layers for efficient and stable perovskite solar cells with a high fill factor and eliminated hysteresis. *J Mater Chem A Mater* 7:26421–26428. <https://doi.org/10.1039/C9TA08314F>
- Dutta Majumdar J, Manna I (2011) Laser material processing. *Int Mater Rev* 56:341–388. <https://doi.org/10.1179/1743280411Y.0000000003>
- Lambiase F, Genna S (2018) Laser assisted joining of AA5053 aluminum alloy with polyvinyl chloride (PVC). *Opt Laser Technol* 107:80–88. <https://doi.org/10.1016/j.optlastec.2018.05.023>
- Huang Y, Gao X, Zhang Y, Ma B (2022) Laser joining technology of polymer-metal hybrid structures - a review. *J Manuf Process* 79:934–961
- Anwer G, Acherjee B (2022) Laser polymer welding process: fundamentals and advancements. *Mater Today Proc* 61:34–42. <https://doi.org/10.1016/j.matpr.2022.03.307>
- Pereira F, Morais Q (2019) Mechanical strength of thermoplastic polyamide welded by Nd:YAG laser. *Polymers (Basel)* 11:1381. <https://doi.org/10.3390/polym11091381>
- Gisario A, Barletta M, Venettacci S, Veniali F (2015) Progress in tridimensional (3d) laser forming of stainless steel sheets. *Lasers Manuf Mater Process* 2. <https://doi.org/10.1007/s40516-015-0012-5>
- Acherjee B (2021) Laser transmission welding of polymers – a review on welding parameters, quality attributes, process monitoring, and applications. *J Manuf Process* 64:421–443. <https://doi.org/10.1016/j.jmappro.2021.01.022>

26. Acherjee B, Kuar AS, Mitra S, Misra D (2015) Laser transmission welding of polycarbonates: experiments, modeling, and sensitivity analysis. *Int J Adv Manuf Technol* 78:853–861. <https://doi.org/10.1007/S00170-014-6693-7/METRICS>
27. Wang R, Zhai J, Kong H et al (2023) Joining of 304 stainless steel to PET by semiconductor laser conduction welding. *J Mater Res Technol* 27:5729–5738. <https://doi.org/10.1016/j.jmrt.2023.11.004>
28. Elahi MA, Plapper P (2022) The durability of stainless steel-polyamide laser joined assemblies. *Procedia CIRP* 111:475–478. <https://doi.org/10.1016/j.procir.2022.08.073>
29. Wu J, Gao X, Huang Y et al (2023) Parameter optimization and quality analysis of pulsed laser joining of 316L stainless steel and polylactic acid. *Opt Laser Technol* 159:108965. <https://doi.org/10.1016/j.optlastec.2022.108965>
30. Adarsh SJ, Natarajan A (2023) Studies on process parameter optimization and surface modification for joint strength enhancement of laser welded aluminium 5754-polyamide hybrid joints. *Mater Today Commun* 37:107198. <https://doi.org/10.1016/j.mtcomm.2023.107198>
31. Temesi T, Czigany T (2022) Laser-joined aluminium–polypropylene sheets: the effect of the surface preparation of aluminium. *Int J Adv Manuf Technol* 121:6907–6920. <https://doi.org/10.1007/s00170-022-09790-0>
32. PerkinElmer, Inc Measurement of Tg of polypropylene using the double-furnace DSC
33. Mofokeng JP, Luyt AS, Tábi T, Kovács J (2011) Comparison of injection moulded, natural fibre-reinforced composites with PP and PLA as matrices. *J Thermoplast Compos Mater* 25:927–948. <https://doi.org/10.1177/0892705711423291>
34. Blaine RL (2002) Thermal application note. In: *Polymer Heats of Fusion*. Thermal Applications Note
35. Parodi E, Govaert LE, Peters GWM (2017) Glass transition temperature versus structure of polyamide 6: a flash-DSC study. *Thermochim Acta* 657:110–122. <https://doi.org/10.1016/j.tca.2017.09.021>
36. Makhlof A, Layachi A, Kouadri I et al (2020) Structural study and thermal behavior of composites: polyamide 66/glass fibers: the reinforcement ratio effect on the kinetics of crystallization. *J Compos Mater* 54:1467–1481. <https://doi.org/10.1177/0021998319883913>
37. Kong Y, Hay JN (2002) The measurement of the crystallinity of polymers by DSC. *Polymer (Guildf)* 43:3873–3878. [https://doi.org/10.1016/S0032-3861\(02\)00235-5](https://doi.org/10.1016/S0032-3861(02)00235-5)
38. Rittenhouse B, Mi X, Allen C (2019) Beginner’s guide to Twitter data. *Programming Historian*. <https://doi.org/10.46430/phen0083>
39. Kagan VA, Bray RG, Kuhn WP (2002) Laser transmission welding of semi-crystalline thermoplastics-part I: optical characterization of nylon based plastics. *J Reinf Plast Compos* 21:1101–1122. <https://doi.org/10.1177/073168402128987699>
40. Genna S, Leone C, Tagliaferri V (2017) Characterization of laser beam transmission through a high density polyethylene (HDPE) plate. *Opt Laser Technol* 88:61–67. <https://doi.org/10.1016/j.optlastec.2016.08.010>
41. Rodríguez-Vidal E, Sanz C, Soriano C et al (2016) Effect of metal micro-structuring on the mechanical behavior of polymer-metal laser T-joints. *J Mater Process Technol* 229:668–677. <https://doi.org/10.1016/j.jmatprotec.2015.10.026>
42. Miller RG, Brown BW (1997) *Beyond ANOVA: basics of applied statistics*, First edn. Chapman & Hall/CRC
43. Rudzinski S, Häussler L, Harnisch C et al (2011) Glass fibre reinforced polyamide composites: thermal behaviour of sizings. *Compos Part A Appl Sci Manuf* 42:157–164. <https://doi.org/10.1016/j.compositesa.2010.10.018>
44. Pracella M, Rolla L, Chionna D, Galeski A (2002) Compatibilization and properties of poly(ethylene terephthalate)/polyethylene blends based on recycled materials. *Macromol Chem Phys* 203:1473–1485. [https://doi.org/10.1002/1521-3935\(200207\)203:10/11<1473::AID-MACP1473>3.0.CO;2-4](https://doi.org/10.1002/1521-3935(200207)203:10/11<1473::AID-MACP1473>3.0.CO;2-4)
45. Di Siena M, Genna S, Moretti P et al (2023) Study of the laser-material interaction for innovative hybrid structures: thermo-mechanical characterization of polyethylene-based polymers. *Polym Test* 120:107947. <https://doi.org/10.1016/j.polymertesting.2023.107947>
46. Ma Z, Shao C, Wang X et al (2009) Critical stress for drawing-induced  $\alpha$  crystal-mesophase transition in isotactic polypropylene. *Polymer* 50(12):2706–2715. <https://doi.org/10.1016/j.polymer.2009.04.010>
47. Parenteau T, Ausias G, Grohens Y, Pilvin P (2012) Structure, mechanical properties and modelling of polypropylene for different degrees of crystallinity. *Polymer* 53(25):5873–5884. <https://doi.org/10.1016/j.polymer.2012.09.053>
48. Bonten C, Tüchert C (2002) Welding of plastics-introduction into heating by radiation. *J Reinf Plast Compos* 21. <https://doi.org/10.1106/073168402027287>
49. Bachmann FG, Russek UA (2002) Laser welding of polymers using high power diode lasers
50. Acherjee B, Kuar AS, Mitra S, Misra D (2011) Application of grey-based Taguchi method for simultaneous optimization of multiple quality characteristics in laser transmission welding process of thermoplastics. *Int J Adv Manuf Technol* 56:995–1006. <https://doi.org/10.1007/s00170-011-3224-7>
51. Acherjee B (2020) Laser transmission welding of polymers – a review on process fundamentals, material attributes, weldability, and welding techniques. *J Manuf Process* 60:227–246
52. Liu FC, Dong P, Pei X (2020) A high-speed metal-to-polymer direct joining technique and underlying bonding mechanisms. *J Mater Process Technol* 280:116610. <https://doi.org/10.1016/j.jmatprotec.2020.116610>
53. Lambiase F, Paoletti A, Grossi V, Di IA (2017) Friction assisted joining of aluminum and PVC sheets. *J Manuf Process* 29:221–231. <https://doi.org/10.1016/j.jmapro.2017.07.026>
54. Wang X, Liu B, Liu W et al (2017) Investigation on the mechanism and failure mode of laser transmission spot welding using PMMA material for the automotive industry. *Materials* 10:22. <https://doi.org/10.3390/ma10010022>
55. Montgomery DC *Design and analysis of experiments* John Wiley & Sons

**Publisher’s note** Springer Nature remains neutral with regard to jurisdictional claims in published maps and institutional affiliations.

Springer Nature or its licensor (e.g. a society or other partner) holds exclusive rights to this article under a publishing agreement with the author(s) or other rightsholder(s); author self-archiving of the accepted manuscript version of this article is solely governed by the terms of such publishing agreement and applicable law.